npj | Flexible Electronics

www.nature.com/npjflexelectron

ARTICLE OPEN

Check for updates

A flexible ECG patch compatible with NFC RF communication

Mohammad Zulqarnain[1]✉, Stefano Stanzione[2], Ganesh Rathinavel[2,4], Steve Smout[3], Myriam Willegems[3], Kris Myny[3] and Eugenio Cantatore[1]

With the advent of the internet of things, flexible wearable devices are gaining significant research interest, as they are unobtrusive, comfortable to wear and can support continuous observation of physiological signals, helping to monitor wellness or diagnose diseases. Amorphous Indium Gallium Zinc Oxide (a-IGZO) Thin Film Transistors (TFTs) fabricated on flexible substrates are an attractive option to build such bio-signal monitoring systems due to their flexibility, conformability to the human body, and low cost. This paper presents a flexible electrocardiogram (ECG) patch implemented on foil with self-aligned IGZO TFTs, which is capable to acquire the ECG signals, amplify them and convert them to a sequence of bits. The analogue frontend has a measured input-referred noise of 8 μV_{rms} in the 1–100 Hz band. The system achieves experimentally 67.4 dB CMRR, 58.9 dB PSRR, and 16.5 MΩ input impedance at 50 Hz while using 1 kHz chopping. The signal from the electrodes is transformed to a 105.9-kb/s Manchester-encoded serial bit stream which could be sent wirelessly to a smart phone via Near Field Communication (NFC) for further elaboration. Power consumption is 15.4 mW for the digital and 280 µW for the analogue part. This contribution shows the fundamental steps to demonstrate intelligent plasters for biomedical applications based on flexible electronics providing an NFC-compatible digital output bit stream.

npj Flexible Electronics (2020)4:13 ; https://doi.org/10.1038/s41528-020-0077-x

INTRODUCTION

Wearable biomedical devices have witnessed a growing interest in recent years. Indeed, these devices allow long-term non-invasive monitoring of people in the comfort of their daily routine[1–3], providing information that is valuable to enable early diagnosis and effective treatment of patients, or that can be used to support a healthy lifestyle. Biomedical wearables typically aim at measuring vital signs or the bioelectric activity of different organs, such as the brain, the muscles and the heart. These signals will be named in the context of this paper as "bio-signals".

Cardiovascular diseases are worldwide the first cause of death, causing 31% of all fatalities every year[4]. A valuable tool to diagnose these diseases is the electrocardiogram (ECG), a non-invasive surface measurement of the heart's electrical potentials. To perform ECG measurements, patients are generally connected with wires to a bulky biopotential acquisition system. This makes long-term monitoring impossible. Wearable solutions for continuous monitoring of ECG would thus be particularly valuable to diagnose various cardiovascular diseases in an early stage. For this reason, the focus of this work is on a wearable patch to measure ECG.

Continuous monitoring of physiological signals require wearable devices to be conformable to the shape of the body, in order to improve the quality of physiological signal monitoring and to ensure maximum comfort of use. Advancements in fabrication techniques and new materials that make possible to build flexible and conformal electronics are thus an important enabler to build wearables for biomedical applications[5–7].

Many flexible materials including polysilicon[8], hydrogenated amorphous Silicon (a-Si:H)[9], organic semiconductors[10,11], and metal oxides[12] have been investigated to serve as semiconductors in thin film transistors (TFTs) in the last few decades. Hosono's group gave a fundamental contribution to the field of flexible TFTs demonstrating amorphous indium gallium zinc oxide (a-IGZO) TFTs deposited on a flexible polyethylene terephthalate substrate at room temperature[13]. These a-IGZO TFTs[14–16] fabricated on flexible large-area substrates are a very interesting platform to build wearable bio-signal acquisition systems due to their flexibility, lightweight, and low cost.

Present wearable bio-signal monitoring devices can be broadly classified in three categories:

(1) Wearable devices in which all active components are rigid Silicon integrated circuits (ICs). These devices are built by encapsulation and packaging techniques exploiting flexible or elastic layers, by integration in fabrics and/or by using flexible interconnects. These wearables can implement complex electronic functionality thanks to the Silicon ICs, at the cost of a reduced comfort level for the user, due to the presence of many rigid parts. Examples of such IC-based wearables include ECG sensors with electrodes integrated into a cotton T-shirt[17], cardiac sensors where a rigid IC is encapsulated in elastic layers[18,19], stretchable "e-tattoos" for ECG and temperature monitoring[20], and a portable electrocorticography (ECoG) system with flexible microelectrodes array[21]. Multimodal bio-signal acquisition has been demonstrated too, with stretchable sensors capable of monitoring several combinations of electroencephalograpgy (EEG), ECG, electromyography (EMG), electrooculography (EOG), and photoplethysmography (PPG)[22–24].
(2) Wearable devices in which sensors and/or front end elements are based on flexible materials/substrates while the rest of the system is implemented with rigid Silicon ICs. In this type of hybrid solutions, flexible electronic devices

[1]Integrated Circuits Group, Eindhoven University of Technology, Eindhoven, The Netherlands. [2]Holst Centre/imec, Eindhoven, The Netherlands. [3]imec, Leuven, Belgium. [4]Present address: The Mathworks B.V., Eindhoven, The Netherlands. ✉email: m.zulqarnain@tue.nl

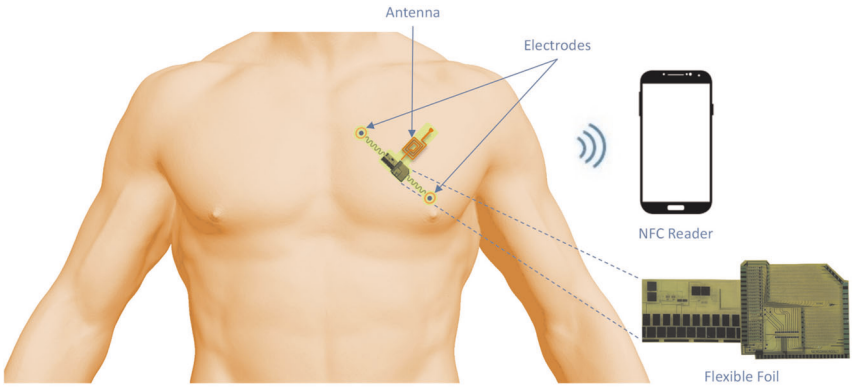

Fig. 1 Application scenario. The presented ECG patch in a representative application scenario.

and sensors are used for interfacing with the human body, while rigid electronics (conventional Silicon ICs) are used for the signal processing and communication functions such as amplification, filtering, digitization and data transmission. In this way, the flexibility and conformability of the flexible substrate are combined with the good signal acquisition and processing capability of rigid components. In this approach, however, the manufacturing steps and costs increase, due to the processing required to combine flexible and rigid parts. Besides, the rigid components may result in reduced patient comfort and in disturbance to the measurements due to movements. Examples of this category of wearable sensors include screen-printed electrodes for ECG[25,26], electrophysiological sensing arrays[27], self-powered ultra-flexible electronics using organic electrochemical transistors[28], implantable sensors for the brain[29], flexible printed electrodes for EEG[30], a pulse oximeter based on organic materials compatible with flexible substrates[31], an ultrasonic device conformable to the skin and capable of monitoring blood pressure[32], and epidermal electronics for multimodal physiological monitoring[33].

(3) Wearable devices in which all components are built using flexible electronics. The materials exploited in these flexible devices are lightweight and fully conformable to human body, ensuring maximum user comfort. Examples of such wearable sensors include flexible ECG monitoring devices[34–36], a prosthetic skin with stretchable multi-electrode arrays for nerve stimulation[37], organic electrochemical transistors for ECoG monitoring[38], large-area flexible or stretchable sensors able to detect arterial pulses[39,40], and an epidermal electronic system capable of monitoring ECG and EMG[41]. Although all these examples show the feasibility of flexible or conformable wearable devices, the inherently poor electric performance of flexible TFT technologies results in limited electronic functionality for this class of wearables. For instance, all smart bio-signal sensors based only on flexible components lack digitization of the measured signals and data transmission capability[34–41].

In an effort to advance the state of the art of wearable bio-signal monitoring devices exclusively based on flexible electronics, we report here for the first time (to the best of the authors' knowledge) a flexible ECG sensor which exploits TFT-based circuits on flexible foil for the full chain of signal acquisition, amplification and digitization[34–41] and is capable to measure ECG signals captured by a pair of electrodes with sufficient signal to noise ratio[42] (Fig. 1). Additionally, the digital output is provided as a serial 105.9 kb/s Manchester-encoded bit stream compatible with the NFC wireless transmission standard, so that the measured data could be sent to a smart phone for further elaboration and presentation. The absence of any rigid active component makes the system conformable to the human body and comfortable to use. Moreover, the implementation of the full system with flexible TFTs reduces the extra processing steps and the cost required for the integration of rigid and flexible electronic components, enabling a solution that could become compatible with single use.

RESULTS

System architecture

A biopotential acquisition system typically consists of two main blocks (Fig. 2a): an analogue frontend (AFE) amplifies the signal while ensuring a suitable noise level, to preserve the shape of the signal, and provides sufficiently high impedance to enable reading the voltage present on the skin with appropriate electrodes. An analogue to digital converter (ADC) follows, to convert the biopotential signal to a digital representation, enabling robust wireless transmission and/or further signal processing. As shown in Fig. 2a, the ADC consists typically of a comparator, a digital to analogue converter (DAC) and suitable logic. To minimize the influence of temperature and technology variability, both the AFE and the ADC are typically designed so that their signal transfer function is determined by the ratio of similar components (e.g. resistors). If variations affect all components proportionally to their value (e.g. the resistance per square increases by a given amount), these ratios tend to stay unchanged. Moreover, in typical Silicon designs, the DAC uses a reference voltage generator (Fig. 2a). This reference voltage is very stable against process, supply and temperature (PVT) variations. The DAC uses this reference to produce output voltages that are also stable against PVT. At the state of the art, it is difficult to make a voltage reference in a-IGZO, because the main components used for this purpose (diodes and bipolar junction transistors) are not available in a-IGZO processes.

For this reason, the design presented in this paper takes a radically different approach, and digitizes the input data in the time domain. The concept is shown in Fig. 2b. After the AFE a reset integrator is used to transform the signal amplitude in duty cycle information (pulse-width modulated, i.e. PWM representation). This means that the duty cycle of the signal produced by the integrator is proportional to the input signal. Digitization is then simply achieved by counting for how many clock cycles the integrator output is high every period. In this case a time reference is needed for digitization, as shown in Fig. 2b. A time reference can be easily generated in our system, which is meant to communicate to a smart phone via NFC. Indeed the NFC carrier can be received on foil and its 13.56 MHz frequency used as time reference, after suitable division in the digital domain[43].The approach here described provides a robust digitization strategy, without the need for a voltage reference, and thus is particularly suited to implementation with a-IGZO TFTs on foil.

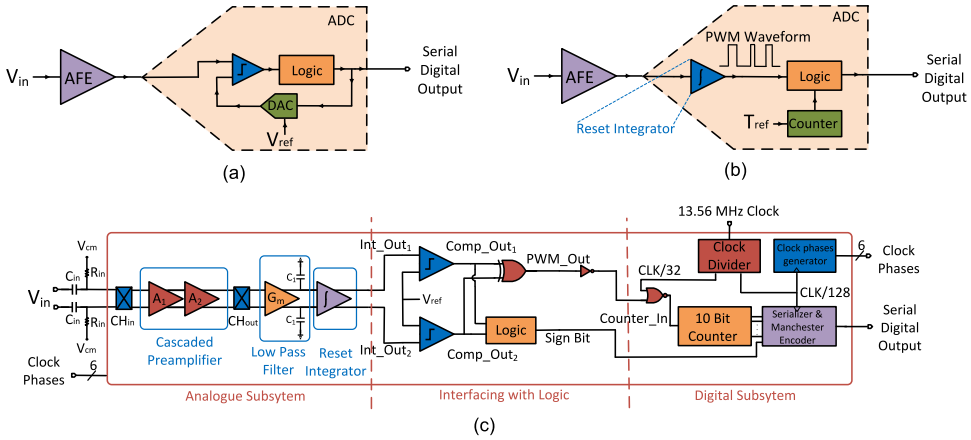

Fig. 2 System architecture. a Conventional biopotential acquisition system, **b** System-level diagram of the ECG acquisition system presented in this work, and **c** Detailed architecture of the presented system.

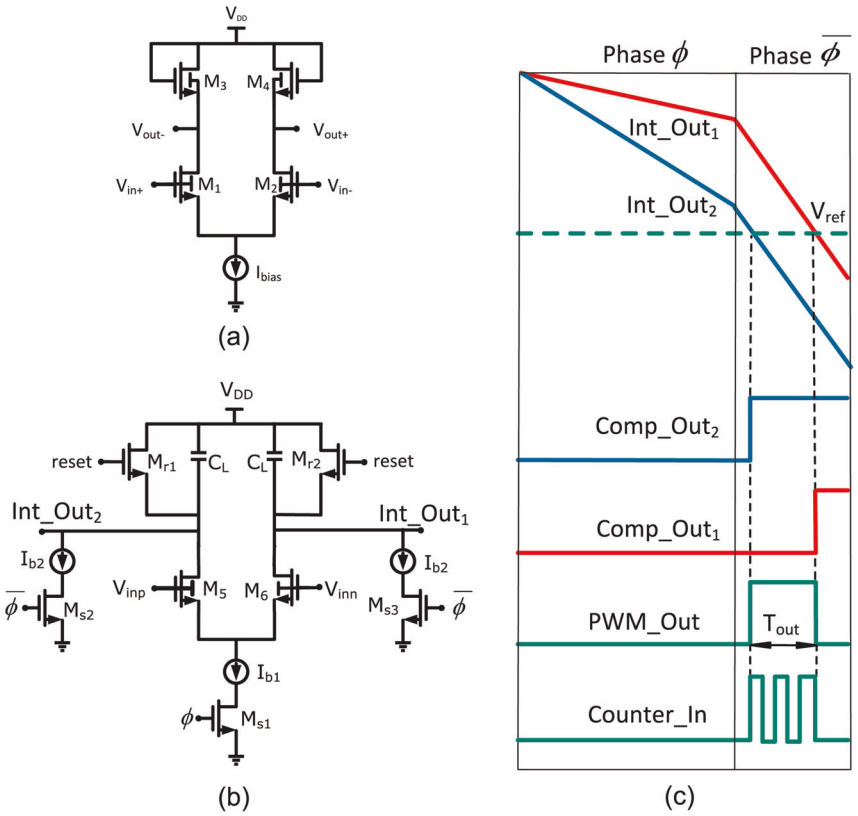

Fig. 3 Circuit schematics and working principle. a Schematics of each of the two cascaded diode-load amplifiers in the preamplifier, **b** Reset integrator, and **c** Reset integrator working principle.

Circuit design

A more detailed schematic of the proposed flexible patch is provided in Fig. 2c. The system consists of two plastic foils (Fig. 1) on which a-IGZO TFTs are fabricated. The first foil (analogue subsystem) is connected to the electrodes. The AFE captures the ECG signals, and the reset integrator transforms them to a PWM representation. The second foil (digital subsystem), connected to the first one (analogue subsystem), digitizes the PWM signal and serializes the output bits, so that they can be sent to a receiver using radiofrequency (RF) NFC communication.

The analogue frontend (AFE) consists of an input chopper (Fig. 2c, CH_{in}), a two-stage cascaded diode connected load preamplifier (Fig. 2c), a de-chopper (Fig. 2c, CH_{out}), and a low-pass filter (Fig. 2c, LPF). The input signal is AC-coupled before the input chopper, to cancel the large DC electrode offsets[44]. Due to the low-frequency bio-signals, chopping is used to supress the amplifier flicker noise and offset. The chopping frequency is chosen as a trade-off between noise, preamplifier bandwidth (which has an impact on power consumption) and input impedance. The preamplifiers are designed to have a bandwidth larger than the target chopping frequency, which is 1 kHz. They are built using diode-connected load TFTs, so that their gain is depending on the ratio of the transconductance of input and load devices, improving the robustness to process variations. The detailed schematics of

each preamplifier is shown in Fig. 3a. The input TFTs $M_{1,2}$ have large (15,000 μm^2) area to bring the 1/f noise corner close to the chopping frequency. For the diode load transistors M_3 and M_4 (Fig. 3a), the back gates are connected to the output nodes to increase the output resistance, while the input transistors M_1 and M_2 have back gates connected to their front gates to increase transconductance and improve noise efficiency. To avoid excessive noise aliasing, the output of the preamplifier is low-pass filtered by another differential amplifier with diode connected load, which has a nominal 100 Hz bandwidth (Fig. 2c, LPF).

The AFE is followed by the reset integrator (Fig. 3b). The latter consists of a differential input pair $M_{5,6}$ with load capacitors C_L. Here a two-phase integration, where in the first phase ϕ the capacitor discharge is signal-dependent, and in the second phase $\overline{\phi}$ the capacitors are discharged by a constant current, is applied (Fig. 3c). The instants at which the integrator outputs are discharged below a given threshold V_{ref} is detected by two external comparators. Thanks to the constant slope observed in the phase $\overline{\phi}$ the time walk difference between the two comparators is minimized and the linearity of the voltage to duty-cycle transformation is improved. Besides, the low-pass behavior of the reset integrator improves the signal to noise ratio of the whole chain. The time delay in threshold crossing between the two branches of the integrator output, T_{out}, is proportional to the input signal (Fig. 3c). The comparator outputs are then fed to a XOR gate to obtain a PWM representation of the input signal with an additional sign bit. The entire analogue subsystem is extremely minimalistic in terms of transistor count, which benefits to the circuit yield and to the power consumption.

From Fig. 3c we can find the relationship between the pulse width of the integrator output, T_{out} and the input signal V_{in}, as:

$$\frac{T_{out}}{V_{in}} = \frac{Ag_m\phi}{I_{b2}} \quad (1)$$

where, T_{out} is the output pulse width, V_{in} the differential input signal, A the gain of the two stage cascaded amplifier, g_m the transconductance of the input transistor in the integrator, ϕ the integration period, and I_{b2} is the discharging current during the phase $\overline{\phi}$.

In the digital subsystem (Fig. 2c), a clock divider is used to generate timing signals from a 13.56-MHz source (CLK). The PWM output is clock gated (and thus quantized in time) with a clock of frequency CLK/32 and then fed to an asynchronous counter which creates a digital multi-bit representation of the PWM output. The typical ECG signal has an amplitude of 1 mV, the target equivalent input noise is in the order of 10 μV$_{rms}$. Adding a margin of 10 dB to make sure that the quantization noise is non-dominant, and additional 10 dB to accommodate for larger signals, one obtains a target dynamic range for the analogue to digital conversion of 60 dB. This necessitates a 10-bit conversion resolution and hence a 10-bit counter has been selected for our first prototype. The counter outputs are then serialized and Manchester-encoded, generating a 32-bit serial stream including a 12-bit preamble, 10 counter bits and other fixed payload. The serializer and Manchester encoder are driven with a clock of frequency CLK/128, to provide the 105.9 kb/s output bit stream which is compatible with NFC RF transmission. The clock phases needed to drive the analogue subsystem are also generated on foil (Clock Phase Generator).

Electrical characterization

Figure 4a shows the measured transfer curve of the cascaded preamplifier. It achieves a gain of 23.5 dB in 3.7 kHz bandwidth with 12.5 μA current consumption from 10 V supply. The integrated input-referred noise in the 1–100-Hz BW is 8 μV$_{rms}$ with a chopping frequency of 1 kHz.

Figure 4b shows the measured transfer curve of the full analogue chain, including the reset integrator and PWM generation. The low frequency gain is 31.3 ms/V. Notice that the notches are at multiples of the inverse of the integration period (555 Hz)

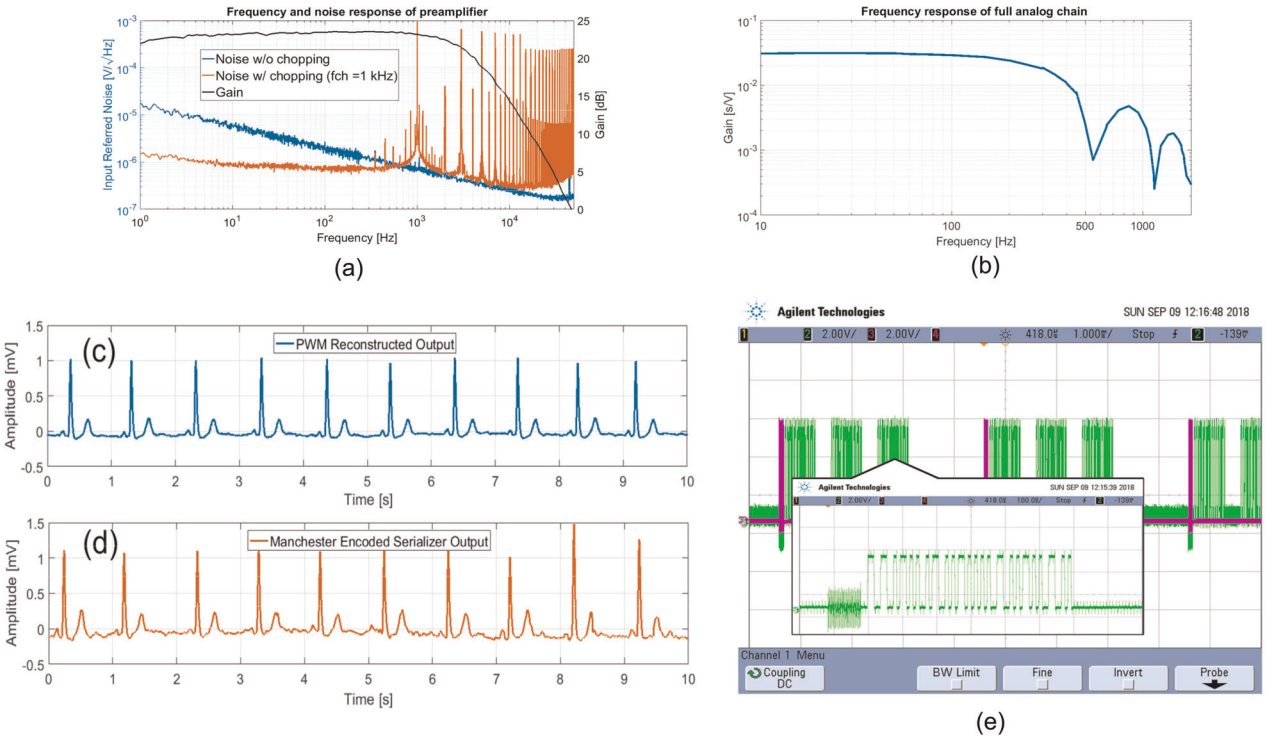

Fig. 4 Measurement results. a Measured frequency response and input-referred noise of the cascaded preamplifier, **b** Measured transfer function of the full analogue chain (from Input to Output PWM), **c** In vivo ECG measured signal reconstructed from the output PWM, **d** In vivo ECG measured signal reconstructed from Manchester Encoded output, **e** Manchester Encoded output corresponding to three samples of the in vivo measurement and a zoom-in of the Manchester encoding of the output bits.

and thus do not affect the target signal bandwidth. The system is powered using a battery and the total power consumption of the analogue front end is 280 µW from a 10 V supply while it is 15.4 mW for the digital subsystem. The system achieves experimentally 67.4 dB CMRR, 58.9 dB PSRR, and 16.5 MΩ input impedance at 50 Hz with 1 kHz chopping. The achieved spurious free dynamic range (SFDR) is 43.11 dB (Supplementary Fig. 1). The linear relationship between the digital code measured at the output of the digital part and the PWM pulse width is shown in Supplementary Fig. 2.

In vivo characterization

Figure 4c shows an in vivo experiment measuring the cardiac activity of a person, obtained by connecting our system to the test subject using standard wet electrodes placed on the chest. A third body electrode (which for simplicity is not shown in Fig. 1) acts as reference connected to the ground. The signal obtained by low-pass filtering the output PWM spectrum in the band of 1–200 Hz is displayed in Fig. 4c. Figure 4d shows the reconstructed signal obtained by the Manchester-encoded serial digital output.

In Fig. 4e a segment of the 105.9-kb/s Manchester-encoded bit stream corresponding to the in vivo measurement is displayed. The bit stream corresponding to the digitization of one sample is repeated three times in order to reduce errors in the NFC transmission. The sampling frequency of the input signal is 250 Hz, while the Manchester-encoded bit stream is generated at 105.9 kb/s, hence, there is sufficient time to repeat each sampled value three times.

Figure 5 shows the foil micrograph of the presented system. The total area of the foil is 123.4 mm^2.

DISCUSSION

Table 1 provides a performance summary and comparison to prior literature. This work is the first reported circuit on foil capable to convert a biopotential input to the digital domain. Additionally, it generates a 105.9-kb/s Manchester-encoded bit stream compatible with the NFC standard. Some of the initial steps taken in the direction of bio-signal acquisition systems using flexible TFT technologies have been published in literature for EEG[45], EMG[46,47], ECG[48] and Heart Rate (HR)[49] measurements. Comparing our contribution to existing literature on flexible TFTs circuits, in references[45–48] the signal is not digitized. A recently published frontend[48] is able to acquire ECG using a flexible TFT-based amplifier, but it also does not digitize the signal. An HR readout on flexible foil[49] was able to convert the signal to binary levels, encoding it in the transition times (i.e. PWM output representation), but was lacking a time-sampled digital output representation (i.e. in bits), which is needed to be compatible with most modern wireless transmission systems. Compared to[49], we have included in this work a digital subsystem (consisting of a 10 bit counter, serializer with Manchester encoder, clock divider and digital phase generator) which transforms the PWM to a time-sampled digital format. The digital clock signals needed to operate the full system are also generated on the foil. Apart from this, the integrated input noise in[49] was 186.3 μV_{rms} which is too high to perform ECG measurements, enabling only HR measurements. Within the analogue frontend we have thus implemented in the present work a low-pass filter after the cascaded preamplifier, which limits in band noise and noise aliasing, and enables 8 μV_{rms} input equivalent noise in the 1–100-Hz bandwidth: a performance that is now compatible with ECG measurements. The input signal is transformed to PWM without digitization in[50] too, and that circuit does not provide a voltage, but rather a current input, making it unsuited to measure biopotential signals. Biopotential amplifiers are typically characterized by a figure of merit called Noise Efficiency Factor – NEF[51]:

$$\mathrm{NEF} = V_{\mathrm{ni,rms}}\sqrt{\frac{2I_{\mathrm{tot}}}{\pi.U_{\mathrm{T}}.4\mathrm{kT}.\mathrm{BW}}} \quad (2)$$

where, $V_{\mathrm{ni,rms}}$ is the total input-referred noise, I_{tot} is the total supply current of the amplifier, BW is the amplifier −3 dB bandwidth, and U_{T} the thermal voltage. As it can be seen from (2) the NEF does not take into account the supply voltage. For this reason, to compare circuits having a different supply voltage V_{DD}, the Power Efficiency Factor PEF was introduced in[52].

$$\mathrm{PEF} = \mathrm{NEF}^2 V_{\mathrm{DD}} \quad (3)$$

The PEF can be used to characterize the trade-off between noise and power consumption, and can be used to compare the power efficiency of different bio-signal acquisition front-ends operating at different supply voltages. In this work, we achieved experimentally NEF and PEF equal to 109.81 and 1.20×10^5 respectively. These figures provide an improvement of 13 and 86% in NEF and PEF respectively, compared to the best NEF and PEF reported for previous bio-signal acquisition front-ends implemented using flexible TFTs[45]. These advancements are obtained due to both, a better TFT technology and circuit improvements. The self-aligned IGZO technology used in this work has indeed a comparatively lower Hooge factor, thus providing less 1/f noise. Besides, the larger input transconductance obtained thanks to the use of the double gate TFT architecture, benefits the noise and power efficiency of the front-end.

This contribution shows the fundamental steps to demonstrate intelligent plasters for biomedical applications based on flexible electronics which are compatible with the NFC standard. The analogue frontend has a measured input-referred noise of 8 μV_{rms} in the 1–100 Hz band, which is the lowest input-referred noise reported in a-IGZO TFT circuits so far[5–7,47,49,50,53]. The system achieves experimentally 67.4 dB CMRR, 58.9 dB PSRR, and 16.5 MΩ input impedance at 50 Hz with 1 kHz chopping. The output is transformed to the digital domain and provided as a 105.9-kb/s Manchester-encoded serial bit stream. To the best of authors' knowledge, this is the first demonstrated ECG acquisition system in flexible IGZO TFTs on foil providing a digital serial output bit stream compatible with the NFC standard[5–7,45–50,53]. Power consumption is 15.4 mW for the digital and 280 µW for the analogue part. The NEF and PEF are 109.81 and 1.20×10^5 respectively, which are the best values reported to date in literature for IGZO TFT circuits[5–7,45–50,53].

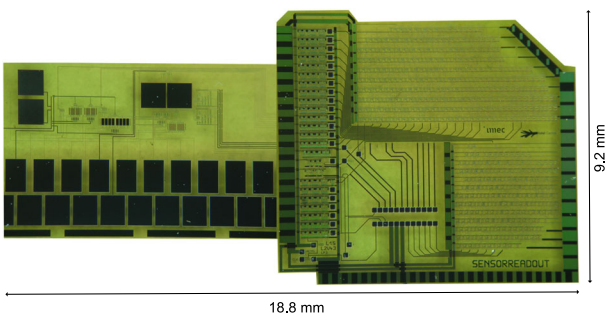

Fig. 5 Foil micrograph. Foil microgrpah of the presented system with dimensions.

METHODS

Technology and TFT electrical characterization

The presented system is fabricated using double gate self-aligned TFTs with a-IGZO[53] as semiconductor, which results in n type TFTs only. The schematic cross-sectional view of a-IGZO TFT is shown in Fig. 6a. The layer stack consists of plastic substrate, a buffer layer, back gate (BG) metal M0, back gate dielectric, a-IGZO, top gate dielectric SiO_2, top gate (TG) metal M1, interlayer dielectric, and source/drain (S/D) metal M2. The fabrication

Table 1. Comparison with the state of the art.

	Moy et al.[45]	Garripoli et al.[50]	Zulqarnain et al.[49]	Garripoli et al.[47]	Sugiyama et al.[48]	This work
Technology	a-Si	a-IGZO	a-IGZO	a-IGZO	DNTT	Dual gate self aligned a-IGZO
Architecture	Chopped amplifier	Asynchronous sigma delta modulator	Chopped amplifier + reset integrator	Chopped amplifier with frequency division multiplexing	Amplifier with AC coupled load	Chopped amplifier + low-pass filter + reset integrator + 10 Bit Counter + serializer with Manchester encoder + clock divider + digital phase generator
Minimum channel length	6 µm	15 µm	15 µm	15 µm	10 µm	1.5 µm
Input domain	Voltage	Current	Voltage	Voltage	Voltage	Voltage
Output type	Analogue	PWM	PWM	Analogue	Analogue	Digital
Application	EEG	Temperature sensor	HR	EMG	ECG	ECG
Chopping frequency	5 kHz	–	500 Hz	5 kHz	–	1 kHz
Integrated noise (BW)	2.3 μV_{rms} (100 Hz)	1.23 nA_{rms} (10 Hz)[a] 4.38 nA_{rms} (300 Hz)[a]	186.3 μV_{rms} (200 Hz)	125 μV_{rms} (500 Hz)	–	8 μV_{rms} (100 Hz)
CMRR	< 50 dB @ 50 Hz	–	–	–	44 dB @ 50 Hz	67.4 dB @ 50 Hz
PSRR	–	–	–	–	–	58.9 dB @ 50 Hz
Input impedance	–	–	–	29 MΩ	–	16.5 MΩ @ 50 Hz
NEF (frontend)	126.29	–	454.29	1534.80	–	109.81
PEF (frontend)	8.77×10^5	–	2.06×10^6	6.12×10^7	–	1.20×10^5
Supply voltage [V]	55	20	10	26	4	10[b] and 5[c]
Power dissipation [mW]	11	2	0.052	1.3	–	0.28[b] + 15.4[c]
Area [mm^2]	–	27.9	52.5	11.2	–	24[b] + 99.3[c]

[a]Calculated from data in Garripoli et al.[47].
[b]Analogue.
[c]Digital.

process starts with the deposition of a buffer layer on a polyimide plastic substrate. Then a BG metal (MoCr) is deposited by physical vapor deposition (PVD). This step is followed by deposition of back gate dielectric (SiO_2) by plasma enhanced chemical vapor deposition (PECVD) at 350 °C. The next step involves the deposition of a-IGZO layer (20 nm with 10% ratio of O_2/Ar) by DC sputtering and patterning with wet etching. After that, the top gate dielectric (SiO_2) is deposited using PECVD at 250 °C, which is followed by TG metal (Mo) layer deposition. Afterwards, the gate stack including metal layer and dielectric is patterned using wet and dry etch in a combined step. Then an interlayer dielectric (SiN_x) is deposited by PECVD at 250 °C. Patterning of contact vias using dry etch follows. In the same step BG, TG and S/D are contacted. The last step involves deposition of S/D (Ti-Al-Ti) metal using PVD and patterning by dry etching. Finally, annealing of the samples takes place at 240 °C in N_2 for 1 h.

The flexible polyimide substrate for the TFT process is hold on glass during manufacturing and released afterwards. The circuits realized in this way can be bent without significantly modifying their electrical characteristics[54].

The transfer characteristics of 43 TFTs, each having aspect ratio of 10/5 (µm/µm), are shown in Fig. 6b. Figure 6c shows threshold voltage (V_T) distribution of these TFTs. The median V_T is −0.36 V while the threshold standard deviation is 0.21 V. Figure 6d shows the mobility distribution of the TFTs, with has a median of 14.47 cm^2/Vs and a standard deviation of 1.30 cm^2/Vs.

Electrical characterization setup

To characterize the preamplifier (Fig. 4a), the device under test has been hooked up via a suitable mechanical connector (Yokowo DS CCNL-050-47-FRC) to off-the-shelf voltage buffers (TI OPA445AP), followed by an instrumentation amplifier (TI INA111AP) for differential to single ended conversion. The output of the instrumentation amplifier is connected to the HP35670A Dynamic Signal Analyser to measure the frequency response and the output noise. A 10-mV_{p-p} sine wave with 5V DC bias, and a 5V DC reference were applied to the positive input (V_{in+}) and negative input (V_{in-}) of the preamplifier (Fig. 3a), respectively. The supply voltage is 10 V. The gain of the preamplifier measured over six samples varied in the range of 23.1–27.5 dB, with a bandwidth between 3.1 and 4.3 kHz, as shown in Supplementary Fig. 3.

For the full analogue chain characterization (Fig. 4b), a 10-mV_{p-p} sine wave with varying frequency was applied to the input of the system and the output PWM was observed. The output data are acquired using a Digilent® Analog Discovery 2 board. The ratio of the fundamental of the filtered output PWM to the applied input provides each point of the frequency response recorded for the full analogue chain (from input to output PWM).

The in vivo measurements are performed connecting our system to the test subject using wet electrodes (Kendall's H124SG) placed on the chest with a spacing of ~5 cm. A third body electrode acts as the ground electrode. The output data are acquired using a Digilent® Analog Discovery 2 board for a period of 10 s. The output spectrum is filtered using MATLAB® with a Butterworth filter in the band 1–200 Hz. The ECG signal is reconstructed by dividing the output signal by the previously recorded full chain gain, to obtain the input referred ECG signal. In vivo measurements from six samples are shown in Supplementary Fig. 4.

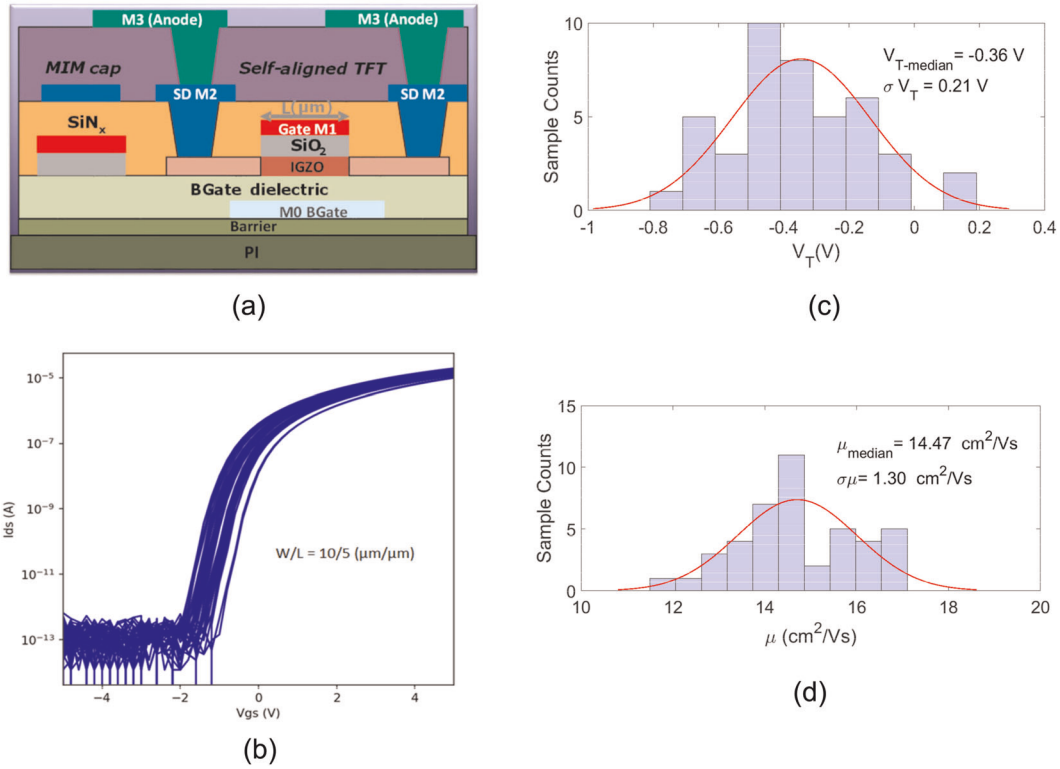

Fig. 6 Device characterization. a TFT cross-sectional view, **b** Id-Vgs transfer curves of TFTs, **c** V_T distribution and, **d** Mobility distribution in a sample of 43 test TFTs.

DATA AVAILABILITY

The experimental data presented in this text is available from the authors upon reasonable request.

Received: 4 August 2019; Accepted: 29 May 2020;
Published online: 15 July 2020

REFERENCES

1. Park, S. & Jayaraman, S. Enhancing the quality of life through wearable technology. *IEEE Eng. Med. Biol. Mag.* **22**, 41–48 (2003).
2. Pantelopoulos, A. & Bourbakis, N. G. A survey on wearable sensor-based systems for health monitoring and prognosis. *IEEE Trans. Syst. Man Cybern.* **40**, 1–10 (2010).
3. Helleputte, N. V. et al. A multi-parameter signal-acquisition SoC for connected personal health applications. In *Proc. 2014 IEEE International Solid-State Circuits Conference Digest of Technical Papers*. 314–315 (2014).
4. World Health Organization. *Cardiovascular diseases (CVDs)*. https://www.who.int/news-room/fact-sheets/detail/cardiovascular-diseases-(cvds).
5. Khan, Y. et al. Monitoring of vital signs with flexible and wearable medical devices. *Adv. Mater.* **28**, 4373–4395 (2016).
6. Khan, Y. et al. Flexible hybrid electronics: direct interfacing of soft and hard electronics for wearable health monitoring. *Adv. Funct. Mater.* **26**, 8764–8775 (2016).
7. Costa, J. C. et al. Flexible sensors—from materials to applications. *Technologies* **7**, 35 (2019).
8. Carey, P. G., Smith, P. M., Theiss, S. D. & Wickboldt, P. Polysilicon thin film transistors fabricated on low temperature plastic substrates. *J. Vac. Sci. Technol. A* **17**, 1946–1949 (2000).
9. Yang, C.-S., Smith, L. L., Arthur, C. B. & Parsons, G. N. Stability of low-temperature amorphous silicon thin film transistors formed on glass and transparent plastic substrates. *J. Vac. Sci. Technol. B* **18**, 683–689 (2000).
10. Dimitrakopoulos, C. D. & Mascaro, D. J. Organic thin-film transistors: a review of recent advances. *IBM J. Res. Dev.* **45**, 11–27 (2001).
11. Dimitrakopoulos, C. D. & Malenfant, P. R. L. Organic thin film transistors for large area electronics. *Adv. Mater.* **14**, 99–117 (2002).
12. Yu, X., Marks, T. J. & Facchetti, A. Metal oxides for optoelectronic applications. *Nat. Mater.* **15**, 383–396 (2016).
13. Nomura, K. et al. Room-temperature fabrication of transparent flexible thin-film transistors using amorphous oxide semiconductors. *Nature* **432**, 488–492 (2004).
14. Barquinha, P., Pereira, L., Goncalves, G., Martins, R. & Fortunato, E. Toward high-performance amorphous GIZO TFTs. *J. Electrochem. Soc.* **156**, H161–H168 (2009).
15. Kim, Y. H. et al. Flexible metal-oxide devices made by room-temperature photochemical activation of sol-gel films. *Nature* **489**, 128–132 (2012).
16. Kim, Y. G. Facile fabrication of wire-type indium gallium zinc oxide thin-film transistors applicable to ultrasensitive flexible sensors. *Sci. Rep.* **8**, 5546 (2018).
17. Nemati, E., Deen, M. J. & Mondal, T. A wireless wearable ECG sensor for long-term applications. *IEEE Commun. Mag.* **50**, 36–43 (2012).
18. Li, Y. et al. A stretchable-hybrid low-power monolithic ECG patch with microfluidic liquid-metal interconnects and stretchable carbon-black nanocomposite electrodes for wearable heart monitoring. *Adv. Electron. Mater.* **5**, 1800463 (2018).
19. Lee, S. P. et al. Highly flexible, wearable, and disposable cardiac biosensors for remote and ambulatory monitoring. *npj Dig. Med.* **1**, 2 (2018).
20. Jeong, H. et al. Modular and reconfigurable wireless E-tattoos for personalized sensing. *Adv. Mater. Technol.* **4**, 1900117 (2019).
21. Xie, K. Portable wireless electrocorticography system with a flexible microelectrodes array for epilepsy treatment. *Sci. Rep.* **7**, 7808 (2017).
22. Xu, S. et al. Soft microfluidic assemblies of sensors, circuits and radios for the skin. *Science* **344**, 70–74 (2014).
23. Jang, K.-I. et al. Self-assembled three dimensional network designs for soft electronics. *Nat. Commun.* **8**, 15894 (2017).
24. Chung, H. U. et al. Binodal, wireless epidermal electronic systems with in-sensor analytics for neonatal intensive care. *Science* **363**, eaau0780 (2019).
25. Imani, S. et al. A wearable chemical–electrophysiological hybrid biosensing system for real-time health and fitness monitoring. *Nat. Commun.* **7**, 11650 (2016).
26. Son, D. et al. An integrated self-healable electronic skin system fabricated via dynamic reconstruction of a nanostructured conducting network. *Nat. Nanotechnol.* **13**, 1057–1065 (2018).
27. Fang, H. et al. Capacitively coupled arrays of multiplexed flexible silicon transistors for long-term cardiac electrophysiology. *Nat. Biomed. Eng.* **1**, 0038 (2017).
28. Park, S. Self-powered ultra-flexible electronics via nano-grating-patterned organic photovoltaics. *Nature* **561**, 516–521 (2018).
29. Kang, S. K. et al. Bioresorbable silicon electronic sensors for the brain. *Nature* **530**, 71–76 (2016).

30. Debener, S., Emkes, R., Vos, M.-D. & Bleichner, M. Unobtrusive ambulatory EEG using a smartphone and flexible printed electrodes around the ear. *Sci. Rep.* **5**, 16743 (2015).
31. Lochner, C. M., Khan, Y., Pierre, A. & Arias, A. C. All-organic optoelectronic sensor for pulse oximetry. *Nat. Commun.* **5**, 5745 (2014).
32. Wang, C. et al. Monitoring of the central blood pressure waveform via a conformal ultrasonic device. *Nat. Biomed. Eng.* **2**, 687–695 (2018).
33. Zhang, Y. & Tao, H. T. Skin-friendly electronics for acquiring human physiological signatures. *Adv. Mater.* **31**, 1905767 (2019).
34. Sekitani, T. et al. Ultraflexible organic amplifier with biocompatible gel electrodes. *Nat. Commun.* **7**, 11425 (2016).
35. Wang, Y. et al. Low-cost, mm-thick, tape-free electronic tattoo sensors with minimized motion and sweat artifacts. *npj Flex. Electron.* **2**, 6 (2018).
36. Koo, J. H. et al. Wearable electrocardiogram monitor using carbon nanotube electronics and color-tunable organic light-emitting diodes. *ACS Nano* **11**, 10032–10041 (2017).
37. Kim, J. et al. Stretchable silicon nanoribbon electronics for skin prosthesis. *Nat. Commun.* **5**, 5747 (2014).
38. Khodagholy, D. et al. In vivo recordings of brain activity using organic transistors. *Nat. Commun.* **4**, 1575 (2013).
39. Wang, X., Gu, Y., Xiong, Z., Cui, Z. & Zhang, T. Silk-molded flexible, ultrasensitive, and highly stable electronic skin for monitoring human physiological signals. *Adv. Mater.* **26**, 1336–1342 (2013).
40. Wang, S. et al. Skin electronics from scalable fabrication of an intrinsically stretchable transistor array. *Nature* **555**, 83–88 (2018).
41. Yeo, W. H. et al. Multifunctional epidermal electronics printed directly onto the skin. *Adv. Mater.* **25**, 2773–2778 (2013).
42. Webster, J. *Medical Instrumentation: Application and Design* (John Wiley & Sons, Hoboken, NJ, USA, 2010).
43. Myny, K. et al. A flexible ISO14443-a compliant 7.5 mW 128b metal-oxide NFC barcode tag with direct clock division circuit from 13.56 MHz carrier. In *Proc. 2017 IEEE International Solid-State Circuits Conference.* 258–259 (2017).
44. Neuman, M. R. *The Biomedical Engineering Handbook: Medical Devices and Systems* (CRC Press, Boca Raton, FL, USA, 2006).
45. Moy, T. et al. An EEG acquisition and biomarker-extraction system using low-noise-amplifier and compressive-sensing circuits based on flexible, thin-film electronics. *IEEE J. Solid-State Circuits* **52**, 309–321 (2017).
46. Fuketa, H. et al. 1 μm-thickness ultra-flexible and high electrode-density surface electromyogram measurement sheet with 2 V organic transistors for prosthetic hand control. *IEEE Trans. Biomed. Circuits Syst.* **8**, 824–833 (2014).
47. Garripoli, C. et al. A fully integrated 11.2 mm^2 a-IGZO EMG front-end circuit on flexible substrate achieving up to 41dB SNR and 29MΩ input impedance. *IEEE Solid-State Circuits Lett.* **1**, 142–145 (2018).
48. Sugiyama, M. et al. An ultraflexible organic differential amplifier for recording electrocardiograms. *Nat. Electron.* **2**, 351–360 (2019).
49. Zulqarnain, M. et al. A 52 μW heart-rate measurement interface fabricated on a flexible foil with a-IGZO TFTs. In *Proc. IEEE 44th European Solid State Circuits Conference.* 222–225 (2018).
50. Garripoli, C. et al. An a-IGZO asynchronous delta sigma modulator on foil achieving up to 43dB SNR and 40dB SNDR in 300Hz bandwidth. In *Proc. 2017 IEEE International Solid-State Circuits Conference.* 260–261 (2017).
51. Steyaert, M., Sansen, W. & Zhongyuan, C. A micropower low-noise monolithic instrumentation amplifier for medical purposes. *IEEE J. Solid State Circuits* **22**, 1163–1168 (1987).
52. Muller, R., Gambini, S. & Rabaey, J. A 0.013 mm^2, 5 μW, DC-coupled neural signal acquisition IC with 0.5 V supply. *IEEE J. Solid-State Circuits* **47**, 232–243 (2012).
53. Myny, K. The development of flexible integrated circuits based on thin-film transistors. *Nat. Electron.* **1**, 30–39 (2018).
54. Tripathi, A. K., Myny, K., Hou, B., Wezenberg, K. & Gelinck, G. H. Electrical characterization of flexible InGaZnO transistors and 8-b transponder chip down to a bending radius of 2 mm. *IEEE Trans. Elect. Dev.* **62**, 4063–4068 (2015).

ACKNOWLEDGEMENTS

K.M. would like to acknowledge funding from the European Research Council (ERC) under the European Union's Horizon 2020 research and innovation programme (Grant Agreement No 716426 - FLICs project). E.C. and M.Z. would like to acknowledge financial support from imec-NL/Holst Centre for the project "Integrated Circuits for Conformal Wearable Systems" and from the TUe/UMC Alliance for the project UEBIT. M.Z. would like to thank Nick van Helleputte for his valuable suggestions.

AUTHOR CONTRIBUTIONS

The overall research was designed and supervised by E.C. and S.S.[2]; the fabrication process was carried out by S.S.[4] and M.W.; the device characterization experiments were carried out by K.M.; the electrical characterization experiments were performed by M.Z., K.M., and G.R.; M.Z. contributed to the signal recording and analysis.; M.Z. wrote the first draft of the manuscript; editing and revision were carried out by E.C., S.S.[2], and M.Z.

COMPETING INTERESTS

The authors declare no competing interests.

ADDITIONAL INFORMATION

Supplementary information is available for this paper at https://doi.org/10.1038/s41528-020-0077-x.

Correspondence and requests for materials should be addressed to M.Z.

Reprints and permission information is available at http://www.nature.com/reprints

Publisher's note Springer Nature remains neutral with regard to jurisdictional claims in published maps and institutional affiliations.